J. Fluid Mech. (1982), *vol.* 123, *pp.* 315–333
Printed in Great Britain

Flow visualization of steady streaming in oscillatory flow through a bifurcating tube

By F. R. HASELTON† AND P. W. SCHERER
Department of Bioengineering, University of Pennsylvania, Philadelphia, Pennsylvania 19104

(Received 26 September 1980 and in revised form 23 March 1982)

A steady streaming displacement of fluid elements is observed to occur during oscillatory flow through a Y-shaped tube bifurcation model at Womersley and Reynolds numbers that can exist in the human bronchial tree. The cause of the displacement is the effect of the asymmetric geometry on the oscillating velocity vector field. The steady streaming displacement is greatest for fluid elements that experience the highest velocity through the bifurcation junction. The maximum displacement observed increases with Re and α up to a Re of about 100 and α of about 5, after which a levelling off and gradual decline occur. Photographs of low-Re and low-α experiments show the effects of secondary components of the steady-streaming displacement field which contribute to a complex circulation.

1. Introduction

Flow through Y-shaped bifurcating tubes is a unique fluid-mechanical feature of mammalian circulatory and respiratory systems, and therefore experimental and theoretical investigation of this flow has attracted the attention of workers in bio-fluid dynamics. Several implications of steady and pulsatile flow in this geometry have been studied. For example, in blood flow, wall shear-stress distribution is thought to influence the site of development of atherosclerosis (Caro, Fitzgerald & Schroter 1969). In the lung, the bifurcation has been shown to be important in bronchial aerosol deposition patterns (Bell 1974), and in the control of the pressure drops along the bronchial tree during inspiration and expiration (Pedley, Schroter & Sudlow 1971). However, the effect of bifurcating tube geometry on purely oscillatory flow, as in the case for air flow in the bronchial tree, has until recently been neglected. These recent results (Haselton & Scherer 1980; Scherer & Haselton 1982) indicate that steady streaming develops in oscillatory flow through a bifurcating tube and that this important fluid-mechanical feature aids in gas exchange with the environment and is a major cause of inhaled aerosol motion. In the following, detailed measurements are presented and discussed for the steady streaming observed in flow visualization experiments conducted in a model of a single bifurcating tube.

The existence of a steady streaming component to oscillatory flow in a planar Y-shaped bifurcation of cylindrical tubes is implied by the differences in the steady-flow velocity vector fields for flow in alternate directions through the bifurcation. Using bifurcation models, measurements of the steady flow fields in the two

† Present Address: Pulmonary Circulation Center, Vanderbilt University, B-1318 – Medical Center North, Nashville, Tennessee 37232.

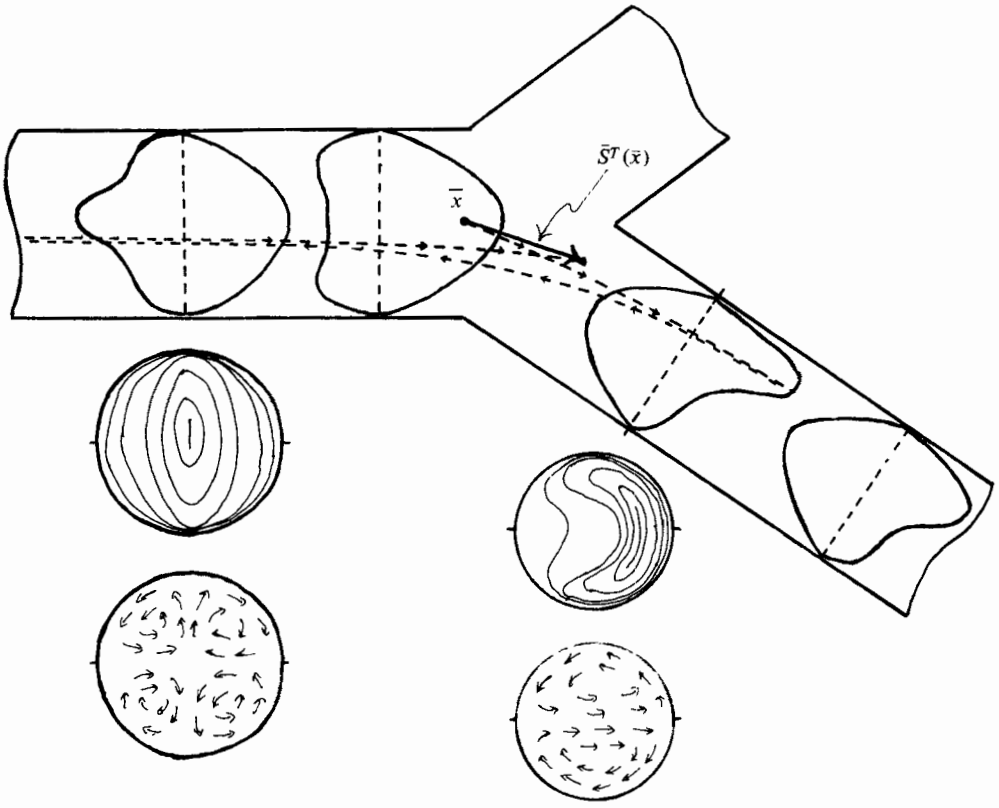

FIGURE 1. Qualitative picture of the steady velocity profiles in a bifurcating tube based on Schroter & Sudlow (1969), Schreck & Mockros (1970), Olson (1971) and Pedley (1977). The profiles shown at four stations within the junction are the axial profiles measured in the plane of the bifurcation. The upper cross-sections shown at a single station for the parent and daughter tubes depict axial-velocity contours. The lower cross-sections illustrate the nature of the secondary components of the velocity field viewed looking towards the junction region, with the right-hand cross-sections for flow from parent to daughter and left-hand for flow from daughter to parent. The dashed line in the tube illustrates the cyclic movement and resulting steady streaming displacement $\bar{S}^T(\bar{x})$ of a fluid element initially at $\bar{x}$.

directions have been made by numerous investigators (Olson 1971; Schreck & Mockros 1970; Schroter & Sudlow 1969), and this work has been thoroughly reviewed by Pedley (Pedley 1977). In general agreement, the results of these studies show that the two steady velocity fields exhibit distinctive properties in the region immediately downstream of the bifurcation. In this region the axial velocity contours over the tube cross section for the steady flow from the single parent into the two daughter tubes exhibit a U-shaped region of high-speed flow (figure 1) displaced near the inside wall of each downstream tube. Swirl components (u_r, u_θ) are observed, which create two regions of helical spiralling motion swirling in opposite directions above and below the plane of bifurcation in the tube. The velocity field observed during steady flow in the opposite direction, that is from the two daughter tubes into the parent tube, is markedly different in the single parent tube immediately downstream of the

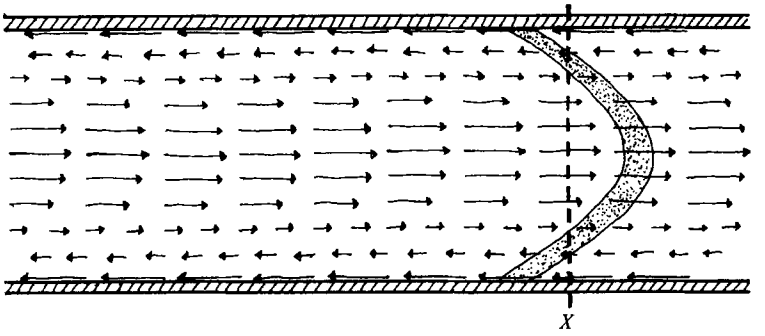

FIGURE 2. Cross-sectional illustration of steady-streaming displacement field in a single straight tube. This displacement field is produced by a hypothetical oscillatory flow whose profiles are parabolic in its flow to the right and flat in its flow to the left. The dotted region is the resulting shape after one cycle of an initially flat plug of traced fluid elements that was uniformly situated across the tube at point X.

bifurcation junction. Axial-velocity profiles in this region exhibit near uniformity across the tube, i.e. they lack the sharp peaks observed in the downstream profiles for flow in the opposite direction but show steep boundary layers at the walls (see figure 1). The angular and radial swirl components of this flow induce a four-celled pattern of spiralling secondary motions. These measurements of steady-flow velocity fields reveal a complex but consistent pattern over the measured range of Reynolds number from approximately 40 to 4500.

In oscillatory flow through a bifurcation, velocity fields similar to these, together with unknown unsteadiness effects, describe the complicated motion of the fluid elements. Although geometric and dynamic complexities of the velocity fields make exact computation impossible at the present time, it is clear that for oscillatory flow, a fluid element will not in general return to its starting position at the end of the flow cycle. This displacement is the resulting steady component of the flow's oscillatory motion, often referred to as steady streaming (Batchelor 1967; Schlichting 1979), and can be defined as

$$\bar{S}^T(\bar{x}) = \int_0^T \bar{u}_p(\bar{x}, t)\, dt, \tag{1}$$

where $\bar{u}_p$ is the Lagrangian velocity experienced by the fluid particle initially at $\bar{x}$, during the flow cycle of period T. The shape of the steady-flow profile measurements suggests that $\bar{S}^T$ would be expected to be non-zero for almost all fluid particles moving through the bifurcation.

In order to introduce several concepts that will prove useful in later discussion, it is convenient to examine first the steady streaming motion of fluid elements in an idealized hypothetical flow. Consider an oscillatory flow, with net volume flux of zero over a flow cycle, in a single, infinitely long straight tube. Let the velocity field during flow to the right be parabolic and in flow to the left, flat or uniform. Figure 2 shows the resultant steady-streaming displacement vector field $\bar{S}^T$ as a function of radial position r for this hypothetical flow. In this example, steady streaming is entirely in the x-direction, and is independent of x. Also shown is the resulting shape of an

initially flat plug of labelled fluid elements that was uniformly situated across the tube at axial position X at the start of the previous flow cycle. The centre of the flat plug has been displaced to the right, in the direction of the parabolic velocity field, and the region near the tube wall has been displaced to the left, in the direction of the flat velocity profile. Each additional cycle of flow would further deform the shape of the tracer-plug bolus by an amount equal to the local steady streaming displacement field. The steady-streaming displacement vector field must satisfy conservation of mass when integrated over any plane normal to the tube axis. This requires that

$$\iint_{R^+} S_x^T \, r \, dr \, d\theta + \iint_{R^-} S_x^T \, r \, dr \, d\theta = 0, \tag{2}$$

where R^+ is the region of the normal plane where the axial component of steady streaming S_x^T is positive, and R^- the region where it is negative. This balanced net streaming can be viewed as a convective exchange of fluid elements across planes normal to the tube axis. A coefficient of this convective-exchange process is conveniently defined for the normal plane at tube position X as

$$CE_X = \iint_{R^+ \text{ or } R^-} S_x^T \, r \, dr \, d\theta / V_T, \tag{3}$$

where V_T is the volume of oscillation in the period T. For this straight-tube hypothetical example, $CE_X = 0{\cdot}25$ for all X.

Since mass transport by convection is of great physiological and medical importance in the function of the respiratory system, and since geometrical complexity of even a single three-dimensional bifurcation precludes much theoretical progress on the problem, a series of flow-visualization experiments was undertaken to gain information and insight into the steady streaming, and resulting convective-exchange process, induced by oscillatory flow through a bifurcating tube.

2. Methods

To investigate steady streaming during oscillatory flow in a bifurcating tube, a flow-visualization experiment was designed to allow direct observation of the movement of labelled fluid elements over a flow cycle. A transparent Plexiglas model of a bifurcating tube was built with approximate geometric similarity to a bronchial bifurcation and large enough to allow easy observation (see e.g. figure 3). All three tubes of the bifurcation were 3·5 cm in inside diameter. The single parent tube was 2 m in length and the two daughter tubes were each 1 m long. The bifurcation junction was bored from a solid block of Plexiglas 5 cm thick, and a tight sleeve fit held the three tubes in a Y-configuration with an angle of 70° between the two daughter tubes. When the parent tube was partially retracted, a 1 cm diameter hole in the parent tube sleeve of the block served as a tracer injection port (see figure 3), but was isolated from the flow when the tube was fully inserted. The model was supported horizontally in a liquid bath.

The fluid within the model was driven by a sinusoidally oscillating pump (Harvard model 613) fitted to the end of the parent tube, and each of the daughter tubes was connected to a separate fluid reservoir open to the atmosphere. The pump could be

adjusted to produce an oscillatory volume of from 0 to 300 cm^3 over a frequency range from 3 to 20 cycles per minute. At the beginning of each experiment, the pump piston was set in mid forward stroke, which is the piston position producing peak fluid velocity, and a bolus of fluid made visible by 20 μm diameter neutrally buoyant white beads was injected via the injection port. The initial position of the 50 cm^3 bolus, though never exactly repeatable, covered the entire cross-section of the tube. The initial position and shape of the bolus were photographed from a camera suspended above the bifurcation with mirrors positioned to provide side views. The pump's oscillation volume and frequency were fixed, and a mechanically tripped switch linked to the pump rephotographed the position and shape of the tracer bolus midway through the forward stroke in each subsequent flow cycle.

Dimensional analysis indicates that the five independent dimensional variables that characterize the steady streaming process (V_T, the oscillation volume (cm^3), f, the frequency of the oscillation (s^{-1}), ν, the kinematic viscosity (cm^2/s), r, the tube radius (cm), and S_x^T, the steady streaming displacement (cm)) can be combined to yield three dimensionless groups. These were chosen to be the Reynolds number, $Re = ur/\nu$, with $u = 2V_T f/\pi r^2$, the non-dimensional frequency parameter of Womersley $\alpha = r(2\pi f/\nu)^{\frac{1}{2}}$, and a non-dimensional streaming displacement $\hat{S} = S_x^T \pi r^2/V_T$. This choice of the non-dimensional form of $\hat{S}$ was made to provide a ratio of steady streaming length to an average path length of a fluid element during a complete flow cycle. The functional dependence among these groups can then be written as

$$\hat{S} = f(Re, \alpha).$$

In order to investigate this functional dependence over a large range of Re and α using a model of fixed size and a pump with a limited range of V_T and f, it is necessary to use several fluids with different viscosities. Changes in viscosity affect both Re and α simultaneously, and the region of the parameter space for f investigated in these experiments was limited to values of α and Re such that α^2/Re was held approximately constant, as is further discussed below.

A fluid viscosity range of 7·0 to 0·01 cm^2/s was achieved by four mixtures of glycerin and water: 99·3 %, 85 %, 65 % and 0 % glycerol as determined by their index of refraction. The fluid-element movements during flow of these mixtures through the model were traced by white beads of approx. 20 μm diameter with $\rho = 1{\cdot}26$ g/cm^3 (Rohm and Haas IRP 64M) for the 99·3 %, 85 % and 65 % glycerol studies, and with beads of $\rho = 0{\cdot}965$ (U.S. Chemical, Microthene F) for the 0 % studies. Using these fluids, the pump generated flows with time-averaged Reynolds numbers from 0·5 to 2000, values of α from 0·3 to 19, and values of α^2/Re ranging from 0·18 to 0·52.

3. Results

It is difficult to observe the steady streaming motion without photographic assistance. To the naked eye, the dominant feature of the experiment is the oscillatory movement of the bead bolus. Direct observation of the injected particle bolus movement during the course of a flow cycle shows that the bolus behaviour during the phases of the fluid flow follows a consistent pattern at all values of Womersley and Reynolds numbers. The tracer beads, which are tightly grouped at the time of injection, are spread axially along the two daughter tubes in an approximate

paraboloid front shape, that is the beads near the centre of the tubes are drawn out farther than those near the tube walls. As the pump piston reaches one end of its stroke, the cloud of beads comes to rest, and the bolus then begins to contract in length, returning to a tightly grouped shape as it passes through the bifurcation at the peak velocity of the fluid flow from the daughter tubes into the parent tube. The bolus is then deformed into another paraboloid shape in the opposite direction as it is drawn into the parent tube. As the pump piston completes its cycle, the bead bolus is again drawn tightly together as it retraces its movement back toward the bifurcation.

Although there is an overall similar motion observed during the flows at all Re and α, the photographs of the bolus cloud as it passes through the bifurcation at the end of the flow cycle when compared sequentially show that the bolus shape deforms as a result of each cycle of flow, and that this deformation is strongly dependent on the values of the Reynolds and Womersley numbers. The entire Re and α range can be divided for convenience of discussion into three subranges, each of which results in a distinct bolus deformation pattern. The photographs of figures 3, 4 and 5 illustrate these patterns which occur in the low Re and α range (Re from 0·5 to 10; α from 0·3 to 1·0), the middle Re and α range (Re from 10 to 200; α from 1·0 to 5·0), and the high Re and α range (Re from 200 to 2000; α from 5·0 to 19). These photographs show the position and shape of the bead cloud at cycles zero, one, four and twenty.

Sequential comparison of the photographs reveals several interesting features of the bolus-deformation process. The most apparent is that throughout the entire range of Re and α the bolus experiences axial steady streaming in both the daughter and parent tubes. For the low α and Re flows the bolus is deformed in much the same way as the bolus injected in the hypothetical straight-tube example. One particle 'tongue' is seen to move down each of the daughter tubes from the centre of the bolus in the parent tube, and two 'tails' are seen to move into the parent tube from the bolus region near the wall (see figure 3*d*). The middle α and Re experiments exhibit similar but less clearly demarcated behaviour, with an evidently higher component of cross-sectional swirl (see figure 4). The high Re and α pattern shows axial streaming, and rapid radial and angular mixing of the beads across the tubes (figure 5*b*).

This difference in mixing that results in variation in bolus uniformity across the tube in the three Re and α ranges is another prominent feature of the photographs. The low Re and α experiments show a very clear and gradual change in bolus deformation, and even after 200 cycles the bolus remains clearly concentrated in distinct regions (figure 9*c*). In the middle Re and α range the bolus undergoes a more rapid deformation, but clearly discernible areas of high bead concentration remain visible over the first 20 cycles (figure 4*d*). The high Re and α flow spreads the beads very rapidly; one cycle being sufficient to completely spread the particles of the bolus uniformly across the tube (figure 5*b*).

A feature common to all three Re and α ranges is that the spreading of the bolus occurs much more rapidly near the bifurcation (in the photographic reference frame), than it does in regions far from the junction. The low Re and α photographs show that bolus deformation per cycle gradually decreases as the bolus front moves away from the bifurcation, and appears to approach an asymptote that limits further spreading. The middle and high Re and α flows show a region of rapid axial spreading near the bifurcation, and a continued, much slower spreading in both axial directions

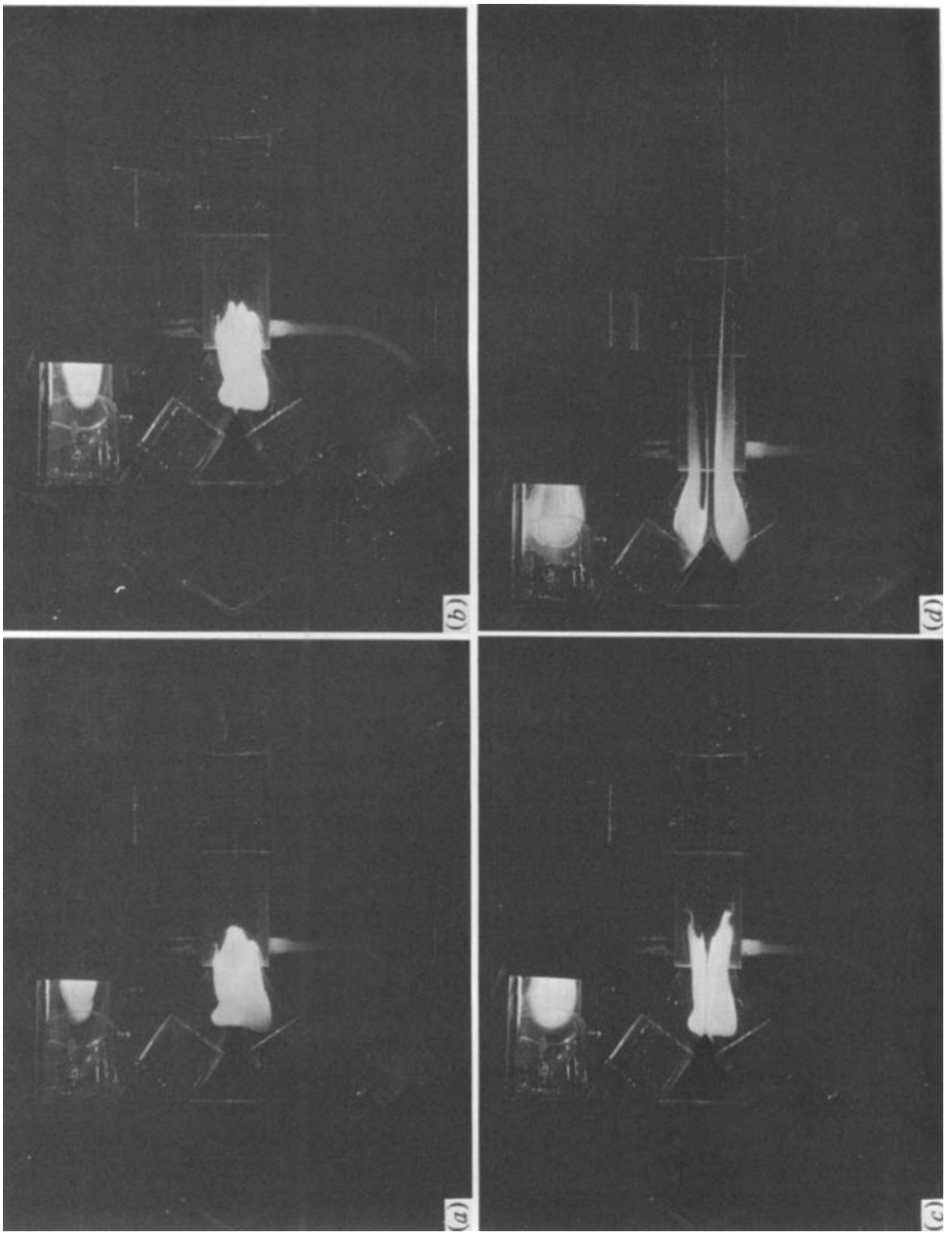

FIGURE 3. Photographs representative of the low α and Re (based on parent-tube radius) experimental range, which show by comparison the steady-streaming displacement of an injected bolus (white in the photographs). The photographs were taken midway through flow to the left at oscillatory flow cycles: (*a*) 0, (*b*) 1, (*c*) 4, (*d*) 20. The volume of oscillation was 300 cm^3 and the frequency $\frac{1}{6}$ cycle/s, which yields a time-averaged Re of 2·6 and $\alpha = 0{\cdot}68$.

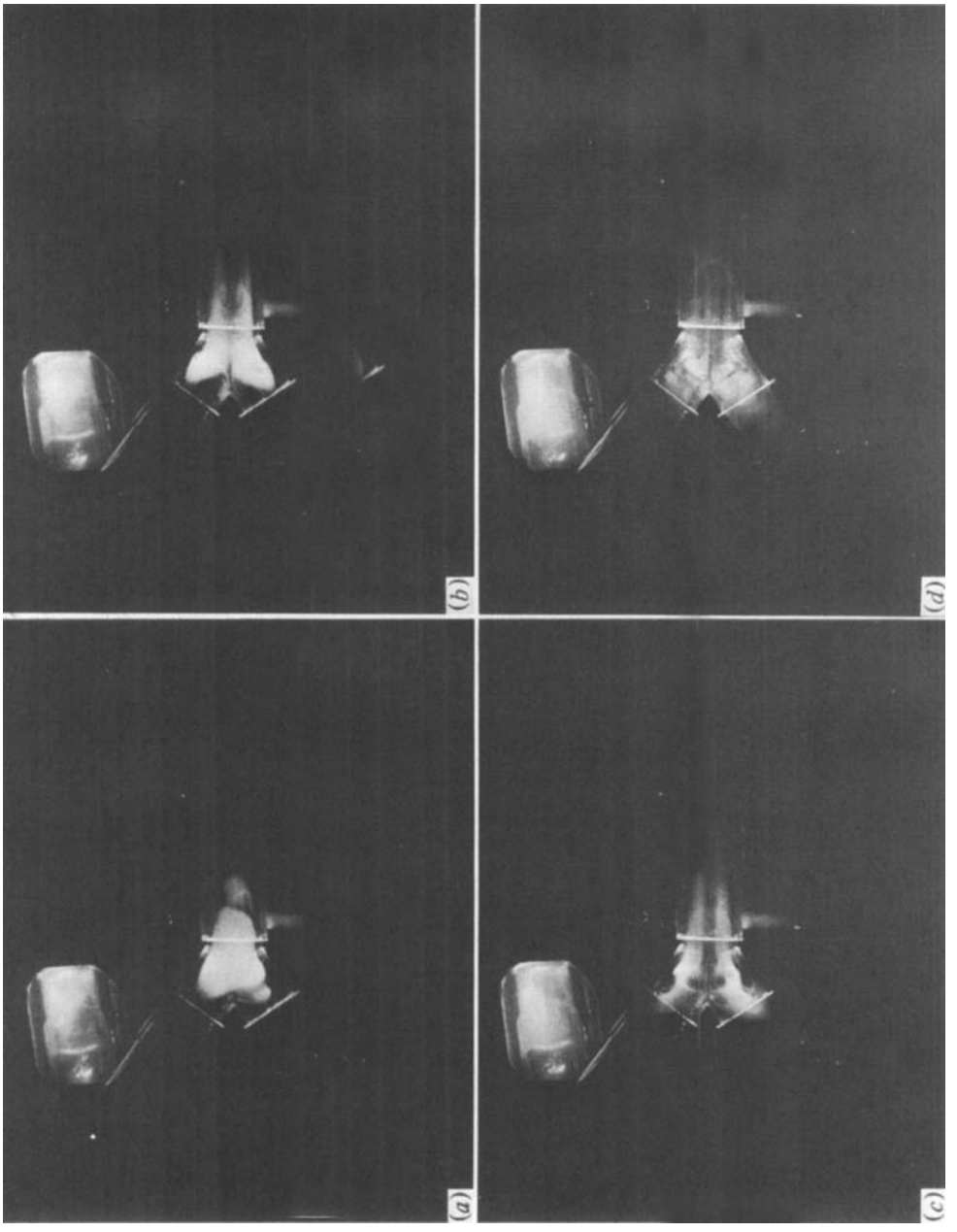

FIGURE 4. Photographs representative of the middle α and Re experimental range taken midway through flow to the left at oscillatory flow cycles: (*a*) 0, (*b*) 1, (*c*) 4, (*d*) 20. The volume of oscillation was 100 cm^3 and the frequency $\frac{1}{6}$ cycle/s, which yields a time-average Re of 44 and $\alpha = 4{\cdot}8$.

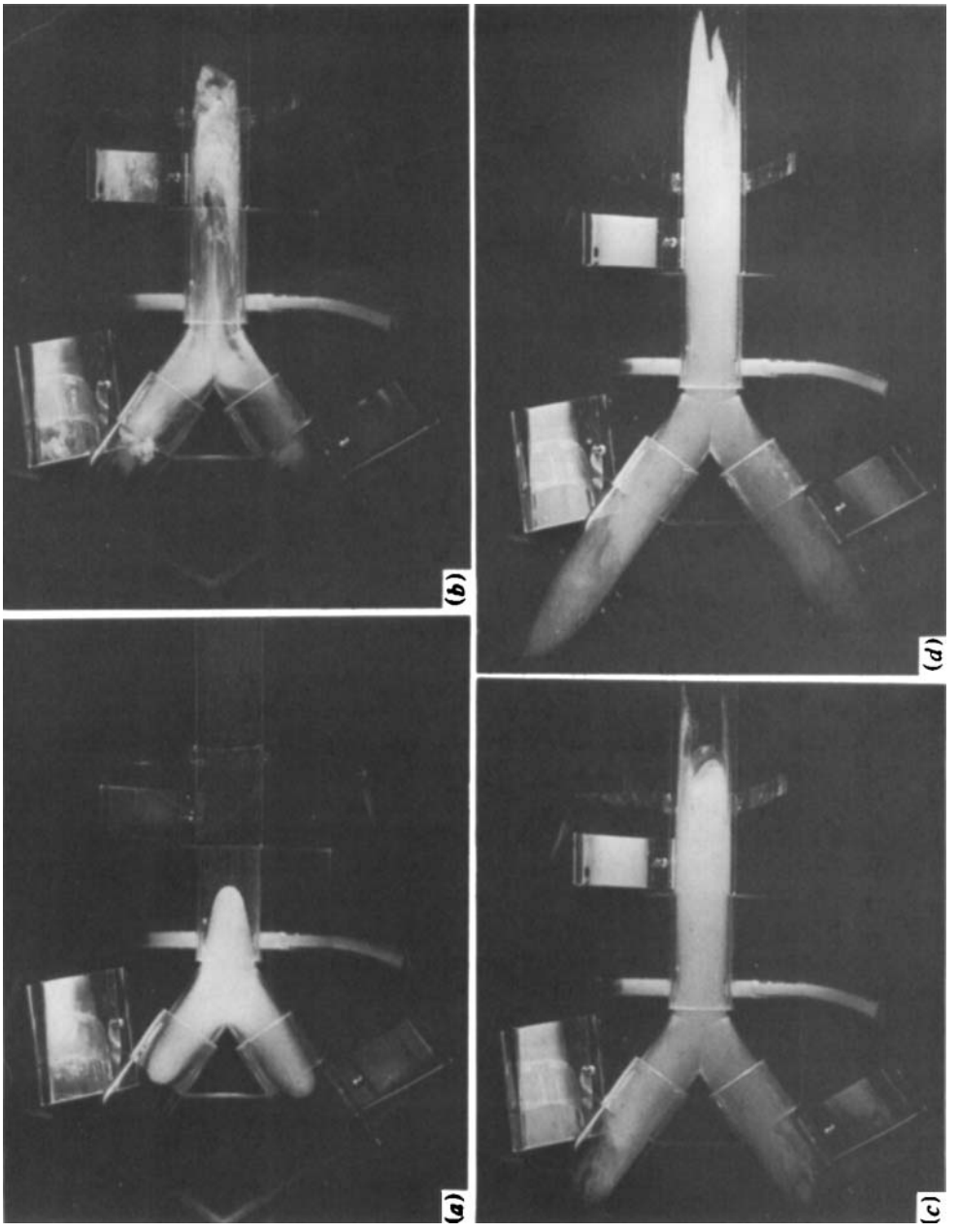

FIGURE 5. Photographs representative of the high α and Re experimental range taken midway through flow to the left at oscillatory flow cycles: (*a*) 0, (*b*) 1, (*c*) 4, (*d*) 20. The volume at oscillation was 200 cm^3 and the frequency $\frac{1}{6}$ cycle/s, which yields a time averaged Re of 1400 and $\alpha = 19$.

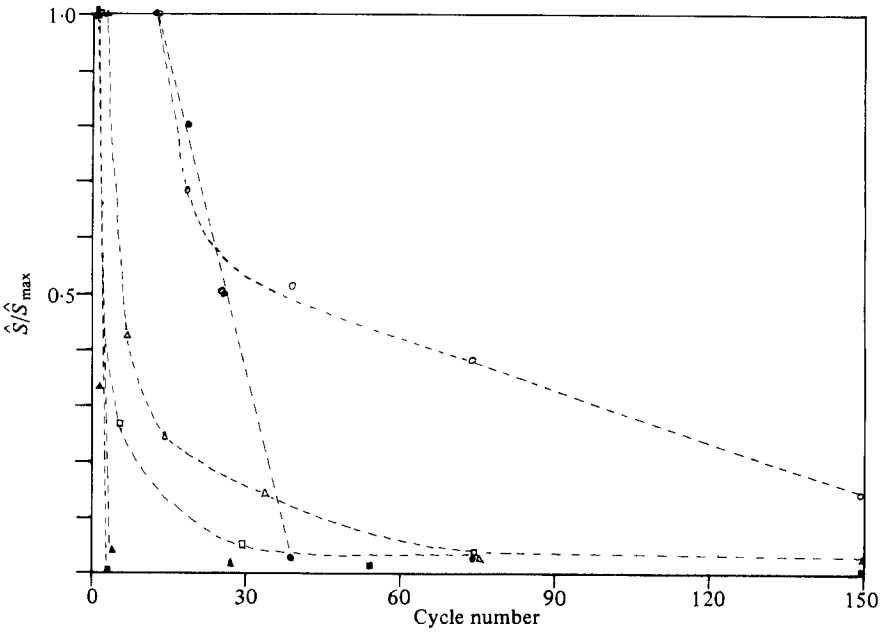

FIGURE 6. The relative magnitude of axial steady-streaming displacements as a function of the number of elapsed cycles of oscillatory flow. Representative curves for the three ranges of α and Re are shown for photographic measurements in the daughter tubes (open symbols) and in the parent tube (filled symbols). The circles show data for $Re = 2{\cdot}6$ and $\alpha = 0{\cdot}68$, the triangles $Re = 44$ and $\alpha = 4{\cdot}8$, and the squares $Re = 2000$ and $\alpha = 19$.

with no apparent limit. Another feature observed at all Re and α is the more rapid spreading of the bolus into the parent tube than into the daughter tubes. The difference is most noticeable in the low and middle Re and α ranges, where it is observed that a sharp peak of the particle tongues spreads rapidly into the parent tube and a more blunted shape spreads gradually into each of the two daughter tubes. This effect is probably due to the fact that the mean longitudinal fluid velocity and Re are higher in the parent tube than in the daughter tubes since the total flow cross-sectional area is smaller. The measurements made from the photographic record discussed below summarize these aspects of the bolus' behaviour over the experimental range of Re and α investigated.

The photographic record was first analysed to determine the position of the bolus peak, that is the point farthest from the tube trisection point, in each of the three tubes for each cycle. Subtraction of these measurements between cycles provided a measure of bolus front displacement $\hat{S}$ in the parent and daughter tubes at various cycles and position. While this experimental measurement of $\hat{S}$ is not obtained by following a single fluid particle over a cycle as required by the theoretical definition given in (1), the identification of local characteristic shapes in the leading edges of the bolus in successive frames indicates that the measurement provides an accurate value of mean displacement of a small cloud of adjacent particles. At high Re and α this identification becomes impossible owing to the high value of the secondary

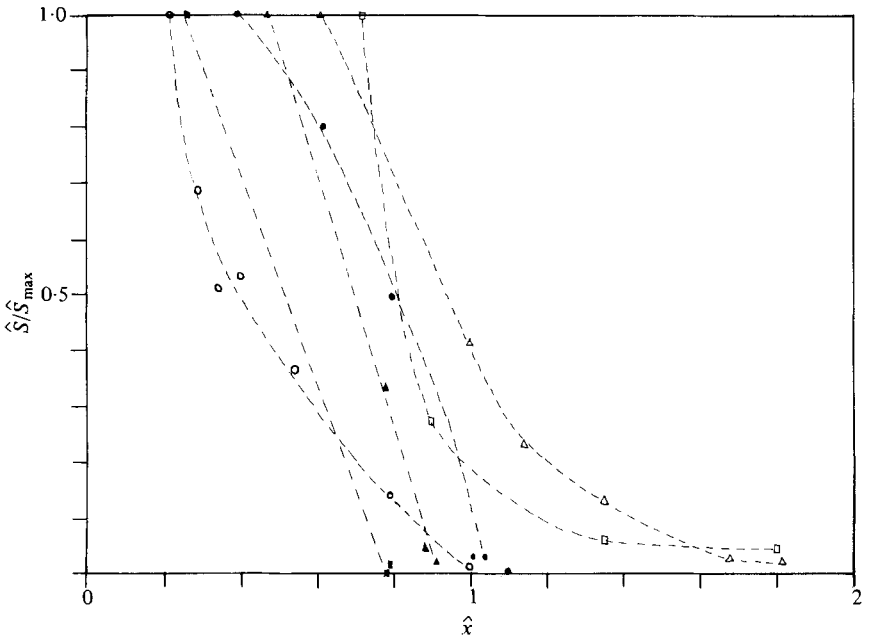

FIGURE 7. The relative magnitude of axial steady-streaming displacement as a function of normalized distance from the trisection of the bifurcation axes. The daughter streaming-displacement measurements (open symbols) and parent streaming displacement measurements (filled symbols) are shown for $Re = 2{\cdot}6$ and $\alpha = 0{\cdot}68$ (circles), $Re = 44$ and $\alpha = 4{\cdot}8$ (triangles), and $Re = 2000$ and $\alpha = 19$ (squares).

components of flow, and the photographic measurement probably underestimates the true value.

To allow comparison of measurements at different Re and α values, the peak $\hat{S}$-value measured, $\hat{S}_{max}$, was used to normalize each set of data. This normalization was used in figure 6 to show the relative components of streaming in the parent and daughter tubes as a function of the average cycle number between measurements for the three α and Re ranges. The peak value of streaming clearly occurs within the first several cycles for parent and daughter streaming at all Re and α. Parent-tube streaming is seen to decline more rapidly than daughter-tube streaming, and the decline in streaming for both tubes occurs much faster at increasing Re and α values. The difference in the rate of decline of $\hat{S}/\hat{S}_{max}$ between the parent and daughter tubes is due to the difference in secondary flow patterns and to a Reynolds number in the parent tube which is twice that in the daughter tube. Since the bolus of beads was initially injected at the peak of the flow velocity through the bifurcation, the decline in $\hat{S}/\hat{S}_{max}$ with cycle number reflects the fact that the tip of the bolus is transiting the bifurcation at lower velocities as it streams to a new position in the oscillatory flow.

Another more direct measure of this behaviour is shown in figure 7. In this graph $\hat{S}/\hat{S}_{max}$ is plotted as a function of $\hat{x}$, the non-dimensional tube distance from the trisection of the bifurcation axes. To permit comparison of $\hat{S}$ at tube positions from

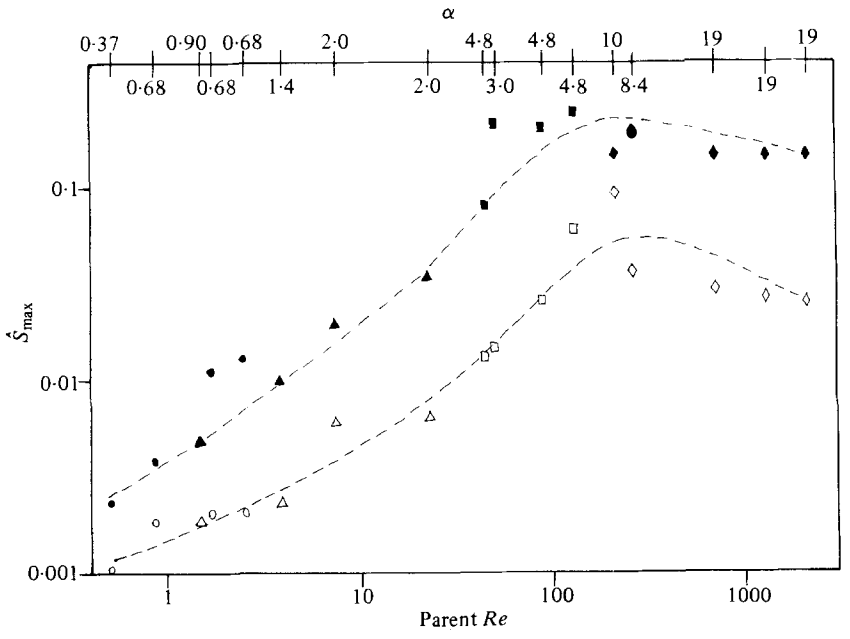

FIGURE 8. The maximum axial steady-streaming displacement as a function of parent-tube time-averaged Reynolds number. The maximum displacement in the daughter tubes (open symbols) and in the parent tube (filled symbols) is shown for the four glycerol–water mixtures: 99·3% glycerol (circles), 85% glycerol (triangles), 65% glycerol (squares), and 0% glycerol (diamonds). The value of α for each data point is indicated on the upper horizontal axis.

experiments conducted at different volumes of oscillation, and to compare directly the streaming between the daughter and parent tubes, the tube position measurements have been normalized by $V_T/2\pi r^2$ for the daughter measurements and by $V_T/\pi r^2$ for the parent-tube measurements. This choice of normalization is discussed further in §4. The graph shows a consistent decline in streaming displacement at tube positions farther from the bifurcation in the photographs. This represents lower streaming displacement for fluid elements that transit the bifurcation at lower velocities. The parent-tube streaming motion falls rapidly toward zero at a normalized distance of less than 1·0, and the decline is steeper for higher values of Re and α. Daughter streaming also falls off around a normalized distance of 1·0, but only in the case of low Re and α does it approach 0 as a limit. For the middle and high Re and α ranges the decline is more gradual to a low, but generally non-zero, value. In all cases the streaming motion is less than 0·05 of the peak value at a normalized distance of 2.

The peak value $\hat{S}_{max}$ of $\hat{S}$, which, as seen in figures 6 and 7, occurs in the first several cycles near the bifurcation, is shown as a function of Re and α in figure 8. The values of $\hat{S}_{max}$ in the daughter tubes and in the parent tube are shown for the Re range of 0·5 to 2020. And the α range of 0·37 to 19. The peak parent-tube streaming is evidently higher at all Re and α values, but both the daughter and parent curves show the same qualitative increase in $\hat{S}_{max}$ with increasing Re up to a Re of 100, after which both curves gradually decline. At low Re the parent $\hat{S}_{max}$ is approximately twice the

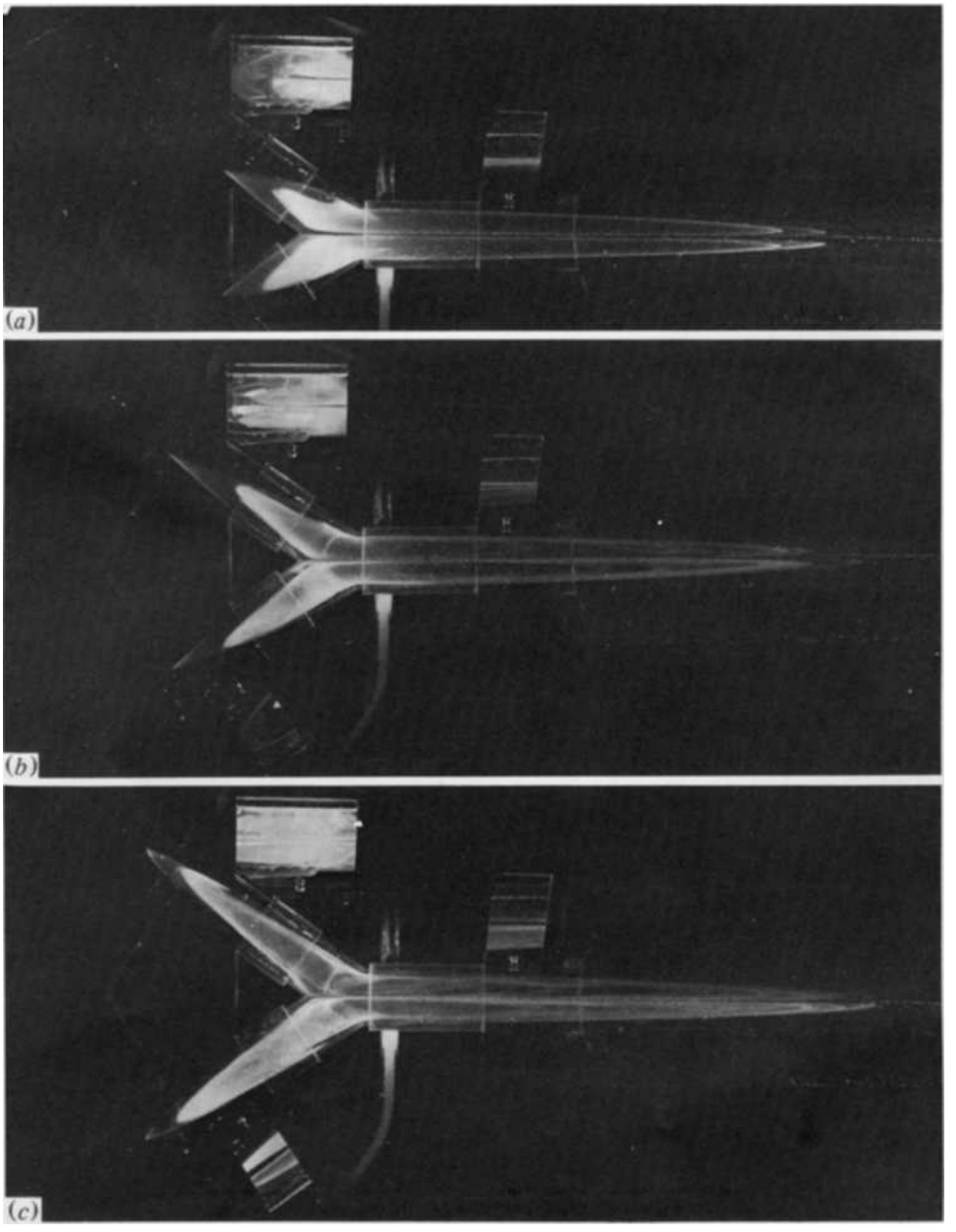

FIGURE 9. Additional photographs of the $Re = 2{\cdot}6$ and $\alpha = 0{\cdot}68$ experiments of figure 3 showing the position of the injected bolus at cycles 50, 100 and 200.

daughter-tube value, but the $\hat{S}_{\max}$ difference increases to almost an order of magnitude at high values of Re. The value of α for each data point, given on the upper horizontal axis, shows that $\hat{S}_{\max}$ increases with α up to an α of about 5, after which $\hat{S}_{\max}$ gradually declines.

Additional cycles of the photographic record shown in figure 3 are contained in figure 9. These photographs are of cycles 50, 100 and 200. Together with figure 3 they show the more rapidly developing axial streaming displacement near the bifurcation, the slow radial and angular steady streaming motion seen as a curling of the bolus above and below the bifurcation plane when viewed in the mirrors, and the slowdown and asymptotically limited behaviour of the axial streaming far from the bifurcation.

4. Discussion

The photographs of the bolus deformations (figures 3, 4, 5, 9), illustrate clearly the steady streaming that is occurring in oscillatory flow through a bifurcating tube. The overall pattern of the steady streaming observed is qualitatively consistent with the published measurements of the steady one-way velocity profiles. This is particularly well-illustrated by the low Re and α flow experiments (figures 3 and 9). The bolus in these photographs deforms down the daughter tubes on the inside wall. As shown in figure 1, this corresponds well with the region of maximum $\hat{S}$ that would be found by superposing the reported axial velocity profiles for steady flow for each of the flow phases in a bifurcating tube. The steady streaming of the bolus in the parent tube occurs near the outside walls, in agreement again with the positions of the expected maximum differences in forward and reverse steady-flow axial-velocity profiles close to the bifurcation as shown in figure 1. The symmetry of the secondary components of the velocity field are equally well illustrated by the four-celled bolus configuration in the low Re and α experiments. The reported measurements of these components in steady flow (Olson 1971; Schreck & Mockros 1970; Schroter & Sudlow 1969) indicate that they always act to induce a spirally motion in the same direction over the entire flow cycle. This consistent direction and spiralling type of motion is seen in the gradual curling of the bolus front above and below the plane of bifurcation. This is most visible in the mirror of the right daughter tube in figures 3(*d*) and 9(*a*). These secondary motions eventually divide the bolus into four distinct cells. This division can be seen by comparing the bolus shape in the side-view mirrors with the overhead view, which shows that the bifurcation plane and its normal in the parent tube are cleared of beads, and that the bead bolus remains in the four-celled pattern that these planes separate.

This type of behaviour is also apparent in the middle Re and α experiments. In the first few cycles the bolus peaks corresponding to the maximum velocity profile differences and the bolus divisions develop more rapidly. However, the division of the bolus into cells is only evident for approximately ten cycles before secondary motions begin to obscure and mix the bolus across the tube, thus blunting the peaks. The high Re and α experiments have a very high component of secondary swirl, and these photographs reveal a highly mixed bolus after only one cycle.

Information about the complete displacement vector field can also be inferred from the photographs of bolus displacement in experiments conducted at low values of Re and α. Conservation of mass over a flow cycle implies that equal fluid volumes must

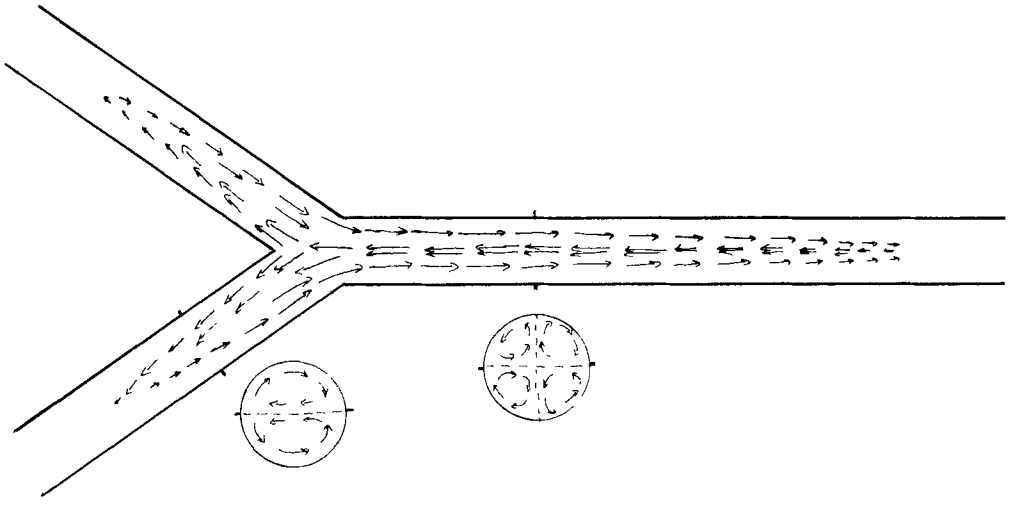

FIGURE 10. Qualitative picture of the complete steady-streaming displacement field for the low α and Re experimental range. The primary axial displacements are sketched in the tube and the secondary displacements in the tube cross-sections looking toward the junction. The straight dashed lines in the tube cross-sections correspond to the regions of flow that become cleared of beads.

be displaced in and out of control volumes bounded by planes across the tubes. At every tube position, the steady streaming displacements measured by the advance of the bolus front away from the bifurcation must then be balanced by oppositely directed steady streaming displacements such that (2) is satisfied. When the photographs of the low Re and α experiments are viewed in sequence, these steady streaming vectors are readily apparent and a qualitative picture of the entire vector field is made evident. Figure 10 is a sketch of the steady-streaming displacement field made from successive frames of the more complete collections of the photographic record from which figures 3 and 9 were selected. Fluid elements are seen to be displaced in the daughter tubes away from the bifurcation near the inside wall and toward the bifurcation near the outside wall. The parent-tube field shows two symmetric regions with streaming displacement vectors away from the bifurcation near the outer wall of the tube and toward the bifurcation in the centre of the tube.

Some insight into the behaviour of the swirl components of the steady-streaming displacement field can also be obtained. A qualitative sketch of S_θ^T and S_r^T is shown in figure 10 at two tube positions. These were inferred from successive frames of the photographic record by comparing the bolus position in the side view mirrors as the experiment progressed. This qualitative sketch represents the maximum information about these components obtainable from these experiments. However, it is interesting to note that this sketch shows the same directional patterns as the secondary velocity profile measurements sketched in figure 1.

Evidently, the secondary displacement components S_θ^T and S_r^T are also functions of distance from the bifurcation. The axial components S_x^T, which contribute to flux across planes normal to the tube axis, have been used to define the convective exchange coefficient CE_X, in (3). Figures 8 and 10 imply the CE_X decrease at tube positions away from the bifurcation and eventually approaches zero far from the

junction. Since locally the steady streaming displacement field is solenoidal, i.e. $\nabla . \bar{\mathbf{S}}^T = 0$, flux balance between neighbouring control volumes, which are bounded by planes across the tube, and which have different CE_X values, must be achieved by the secondary swirl components S_θ^T and S_r^T. Therefore, decreases in CE_X at positions farther away from the bifurcation are balanced by changes in S_θ^T and S_r^T. The overall motion of the fluid elements in the streaming field is composed of primary displacements occurring away from and toward the bifurcation in each tube and secondary displacements in the direction of the secondary velocity components.

An interesting feature of the oscillatory velocity field is shown by the plot of the normalized data in figure 7, which suggests that beyond a characteristic distance from the bifurcation $\hat{S}$ falls rapidly toward zero. However, it known that for steady flow the axial profile velocity measurements in the daughter tubes gradually change from a U-shaped region of high-speed flow (figure 1) to a parabolic flow. Olson's measurements (Olson 1971; Pedley 1977) show that at $Re = 530$ the profile 25 diameters downstream of the bifurcation is still skewed toward the inside wall. Hence forward and backward differences in these velocity profiles far from the junction might result in steady streaming motion as well. The apparent negligible influence of these profiles shown in figure 7 is due to the interaction of the flow's oscillatory nature and the development of velocity profiles whose non-reversibility is a function of distance from the bifurcation.

In an infinitely long straight tube, which would be approximated in tube regions far from the bifurcation, pure oscillatory flow cannot produce steady streaming. This is shown by integrating the linear equation of motion over a cycle to obtain Laplace's equation for the steady-streaming displacement field, $\bar{S}^T$. The boundary conditions of $\bar{S}^T = 0$ at the tube wall and $\bar{S}^T$ finite along the axis imply that the only possible vector field is zero everywhere. Indeed, in similar experiments reported elsewhere (Haselton 1981) no streaming was observed during oscillatory flow in a long straight tube. Neglecting any influence of the tube ends away from the bifurcation, all disturbances to the velocity field that result in steady streaming must originate from the geometry of the bifurcation, and the propagation of the profile disturbance to the otherwise reversible profile at the tube position x must be convected by the fluid. That is, the profiles at x develop reversibly, since locally it is a straight tube until fluid influenced by the bifurcation is convected to that tube position. This suggests that a rather sharp oscillating boundary may exist which separates a steady-streaming region, where $\bar{S}^T \neq 0$, from regions where $\bar{S}^T = 0$ and there is no steady streaming. This boundary oscillates at the front and back of the volume transiting the bifurcation, and by hypothesis just beyond this propagating boundary, i.e. away from the bifurcation the profiles remain reversible.

This hypothesis provides the rationale for plotting the data of figure 7 to show steady streaming as a function of the distance from the bifurcation relative to the position of the postulated reversible front. The normalization factors $V_T/2\pi r^2$ (for the daughter-tube distance measurements) and $V_T/\pi r^2$ (for the parent-tube distances) correspond to the distance from the bifurcation, at the time of the photograph, to the boundary of a reversible front that develops parabolically at the entrance of each tube. With this assumption for the developing shape of the oscillating boundary separating irreversible regions from reversible regions, values of $\hat{x}$ on the horizontal axis that are less than 1 are by hypothesis in a region of the fluid that experiences

irreversible profiles and consequent steady streaming motion. Values greater than 1 on the horizontal axis correspond to a region of the fluid which experiences reversible profiles and no steady streaming. Figure 7 shows that at low Re and α this assumption for the shape of the propagation front seems to be a good one. As $\hat{x}$ increases from 0 to 1·0, the steady streaming falls from its peak value to almost 0. At values above 1·0 there is little if any steady streaming observed. This behaviour occurs in both the parent and daughter tubes. The steady streaming for higher α and Re exhibits a declining value as $\hat{x}$ approaches 1·0; however, unlike the low Re and α case, the daughter steady streaming is observed at values greater than 1. In all cases the value of the steady streaming falls off rapidly at an $\hat{x}$ of approximately 1·0, and approaches nearly zero at larger normalized distances. The more gradual decrease in steady-streaming displacements at $\hat{x}$ greater than 1·0 for the middle and high Re and α ranges is probably due to an oscillating separation boundary that is not developing parabolically but assumes some other shape due to higher components of swirl, greater entrance-length requirements and greater influence of α. The low, constant values of steady streaming far from the bifurcation at middle and high Re and α are thought to be caused by density differences between the injected bolus and the surrounding fluid caused by small temperature differences and high concentration of beads with a slightly different density. A maximum calculated value of streaming can be made based on the simple physical model of a sphere with known radius and density settling at terminal velocity in a time-reversing parabolic velocity field. In these experiments the ratio of the sphere's radius to the tube radius is 5×10^{-4} and the very small force associated with radial migration phenomena is neglected in the calculation (Brenner 1966). The steady-streaming displacement in these regions agrees with this calculated maximum net displacement due to 20 μm diameter particles settling in a tube with oscillating quasi-steady parabolic profiles and a density difference between the particle and the surrounding fluid equal to the density difference in these experiments. The calculation yields an estimate of $\hat{S}/\hat{S}_{\max}$ within 20 % of the experimental value for the middle and high Re and α experimental values. The calculated value of $\hat{S}/\hat{S}_{\max}$ from settling effects for low Re and α is two orders of magnitude lower, in agreement with observed near-zero experimental measurements. The long sloping tongues observed after 200 cycles in the bolus far from the junction in the high Re and α experiments are also in agreement with a density difference effect.

These modelling experiments examine a wide range of coupled values of α and Re with the ratio α^2/Re remaining roughly constant. As such they do not indicate the relative importance of either parameter in producing steady-streaming displacements. However, some remarks may be made about the dependence of $\hat{S}$ on α and Re in extreme regions of the parameter space. As $\alpha \to 0$ steady streaming will still result, at least if $Re > 40$, since the measured steady velocity profiles are known to be different (Schroter & Sudlow 1969). The other extreme of $Re \to 0$ would approach total reversibility independently of the value of α (Slattery 1964), and one would not expect steady streaming to occur. For large enough Re, the flow in either direction would be expected to be turbulent, independently of α, yielding reduced differences in velocity profiles in the two flow directions. For very large α and Re less than necessary for tubulence, the oscillating viscous boundary layer in the straight-tube regions away from the bifurcation is confined to thin layers near the walls. However,

the bolus flow experiences velocity-profile differences due to the inertial forces associated with the flow turning the corner through the bifurcation. These forces would contribute to the secondary components of motion depending on the value of Re, leading to a net displacement.

Thus if $Re \to 0$ independent of α, $\hat{S}$ would be expected to approach zero. While if $\alpha \to 0$ or $\alpha \to \infty$ and Re remains finite, $\hat{S}$ would be expected to vary with Re. These limiting arguments suggest that the streaming is more dependent on Re than on α. However, this conjecture requires further investigation and experiments need to be performed to evaluate the independent functional dependence of $\hat{S}$ on both α and Re.

Limitations in the stroke volume and frequency of the pump prevented varying α and Re independently while covering a large range of either variable. Keeping α^2/Re nearly constant appeared to be the best compromise, and corresponds physiologically at a given bifurcation to varying breathing frequency while keeping the volume inspired per breath constant. Although unaided respiration does not normally occur in this way, the method of high-frequency assisted ventilation currently being actively investigated (Slutsky *et al.* 1980) is often administered in this manner. Also, α^2/Re is roughly constant within the bronchial tree over two-thirds of the bronchial generations forming the upper conductive zone. Keeping α^2/Re constant is equivalent to holding mean particle displacement over a cycle constant while varying frequency or viscosity. The displacement of a given set of particles, however, can be greater or less than the mean. Keeping α^2/Re constant can then be viewed as a way of investigating how inertial effects change the unsteady flow as a function of increasing α which is approximately the same (in the case where $\alpha^2/Re = \text{const}$) as increasing Re.

The same type of steady streaming and convective exchange that has been examined here in some experimental detail for a single symmetric bifurcating tube may also occur in a variety of other geometries. Steady velocity profiles calculated from exact solutions of the Navier–Stokes equations suggest that this same mechanism may operate, for instance, in low-frequency oscillatory flow in a cone, and from a submerged jet. Other unsteady flows whose fluid elements are accelerated in one local geometry and decelerated in another would exhibit similar behaviour, for example pulsatile flow in a diverging channel (Schneck & Walburn 1976).

These experimental results confirm the existence of and provide further insight into the steady streaming and consequent convective-exchange phenomena that occur in oscillatory flow through a single bifurcation at Reynolds and Womersley numbers that can occur in the bronchial tree. These experiments suggest that one important aspect of the design of the bronchial-tree structure is to induce steady-streaming components within the oscillatory flow which assist in the effective convective exchange of gases between the terminal air sacs and the environment, and also strongly affect the transport and site of deposition of inhaled particles.

This research was supported in part by grant HL 20105 from the National Heart and Lung Institute. The authors acknowledge valuable comments and suggestions from the referees.

REFERENCES

BATCHELOR, G. K. 1967 *An Introduction to Fluid Dynamics*, pp. 358–364. Cambridge University Press.

BELL, K. A. 1974 *Aerosol deposition in models of a human lung bifurcation.* Ph.D. thesis, California Institute of Technology.

BRENNER, H. 1966 Hydrodynamic resistance of particles. *Adv. Chem. Engng* **6**, 287–438.

CARO, C. G., FITZGERALD, J. M. & SCHROTER, R. C. 1969 Arterial wall shear and distribution of early atheroma in man. *Nature* **223**, 1159–1161.

HASELTON, F. R. 1981 *Transport and deposition of hygroscopic aerosols in models of the human bronchial tree.* Ph.D. thesis, University of Pennsylvania, Philadelphia.

HASELTON, F. R. & SCHERER, P. W. 1980 Bronchial bifurcations and respiratory mass transport. *Science* **208**, 69–71.

OLSON, D. E. 1971 Fluid mechanics relevant to respiration: flow within curved or elliptical tubes and bifurcating systems. Ph.D. thesis. Imperial College, London.

PEDLEY, T. J. 1977 Pulmonary fluid dynamics. *Ann. Rev. Fluid Mech.* **9**, 229–274.

PEDLEY, T. J., SCHROTER, R. C. & SUDLOW, M. F. 1971 Flow and pressure drops in systems of repeatedly branching tubes. *J. Fluid Mech.* **46**, 365–383.

SCHERER, P. W. & HASELTON, F. R. 1982 Convective exchange in oscillatory flow through bronchial tree models. *J. Appl. Physiol.: Respirat. Environ. Exercise Physiol.* (in press).

SCHLICHTING, H. 1979 *Boundary Layer Theory*, 7th edn, pp. 428–432. McGraw-Hill.

SCHNECK, D. J. & WALBURN, F. J. 1976 Pulsatile blood flow in a channel of small exponential divergence – Part II: steady streaming due to the interaction of viscous effects with convected inertia. *Trans. A.S.M.E.* I: *J. Fluids Engng* **98**, 707–714.

SCHRECK, R. M. & MOCKROS, L. F. 1970 Fluid dynamics in the upper pulmonary airways. *Third Fluid and Plasma Dynamics Conf. Los Angeles: A.I.A.A. Paper* no. 70–788.

SCHROTER, R. C. & SUDLOW, M. F. 1969 Flow patterns in models of the human bronchial airways. *Respir. Physiol.* **7**, 341–355.

SLATTERY, J. C. 1964 Time-reversed flows. *J. Fluid Mechanics* **19**, 625–630.

SLUTSKY, A. S., DRAZEN, J. M., INGRAM, R. H., KAMM, R. D., SHAPIRO, A. H., FREDBERG, J. J., LORING, S. H. & LEHE, J. 1980 Effective pulmonary ventilation with small-volume oscillations at high frequency. *Science* **209**, 609–610.